Nature Environment and Pollution Technology
An International Quarterly Scientific Journal

p-ISSN: 0972-6268
(Print copies up to 2016)
e-ISSN: 2395-3454

Vol. 25 | No. 2 | Article ID B4369 | 2026

Original Research Paper

https://doi.org/10.46488/NEPT.2026.v25i02.B4369

Open Access Journal

Enhancing Photovoltaic (PV) System Efficiency Through Integrated Inclination Control and I-V Curve-Based Diagnostics

S. M. Kamali[1], V. Malathy[2], Ratchagaraja Dhairiyasamy[3]†, Deekshant Varshney[4, 5] and Subhav Singh[6, 7]

[1]Department of Electrical and Electronics Engineering, Annapoorana Engineering College (Autonomous), Periyaseeragapadi, Salem-636308, Tamil Nadu, India

[2]Department of Electronics and Communication Engineering, SR University, Warangal-506371, Telangana, India

[3]Saveetha School of Engineering, Department of Electronics and Communication Engineering, Saveetha Institute of Medical and Technical Sciences, Saveetha University, Chennai, Tamil Nadu, India

[4]Centre of Research Impact and Outcome, Chitkara University, Rajpura-140417, Punjab, India

[5]Noida Institute of Engineering and Technology, 19, Knowledge Park-II, Institutional Area, Greater Noida (U.P.), 201324, India

[6]Division of Research and Development, Lovely Professional University, Punjab, India

[7]Center for Innovation and Inclusive Research, Sharda University, Greater Noida, Uttar Pradesh, India

†Corresponding author: Ratchagaraja Dhairiyasamy; ratchagaraja@gmail.com

Abbreviation: Nat. Env. & Poll. Technol.
Website: www.neptjournal.com

Received: 25-06-2025
Revised: 02-09-2025
Accepted: 04-09-2025

Key Words:

Photovoltaic systems
Supervisory interface
Partial shading analysis
Real-time monitoring
Inclination optimization

Citation for the Paper:

Kamali, S.M., Malathy, V., Dhairiyasamy, R., Varshney, D. and Singh, S. 2026. Enhancing photovoltaic (PV) system efficiency through integrated inclination control and I-V curve-based diagnostics. *Nature Environment and Pollution Technology*, 25(2), B4369. https://doi.org/10.46488/NEPT.2026.v25i02.B4369

Note: From 2025, the journal has adopted the use of Article IDs in citations instead of traditional consecutive page numbers. Each article is now given individual page ranges starting from page 1.

ABSTRACT

Photovoltaic (PV) systems have become central to the global transition toward renewable energy; however, their efficiency is often compromised by environmental variability and inadequate monitoring integration. Therefore, advanced supervisory platforms that unify data acquisition, fault detection, and performance optimization have become increasingly important. Existing monitoring approaches do not adequately integrate grid-connected and isolated systems with real-time diagnostic capabilities. This study was undertaken to develop and validate a supervisory interface capable of simultaneously monitoring multiple PV configurations while incorporating image-based shading detection and tilt optimization. The methodology combined the hardware implementation of rooftop and ground-mounted PV modules, sensor-based data acquisition through LabVIEW, integration with MATLAB/Simulink modeling for system validation, and camera-based analysis for shading and tilt detection. The results demonstrated that shading of a single cell could reduce the total power output by nearly 50%, whereas tilt optimization of approximately 34° increased the energy yield by 14%. The integrated operation of rooftop and ground-mounted systems improved the daily energy output by 11% compared to standalone systems. Statistical analysis confirmed the robustness of these findings, with performance ratio and efficiency indices showing consistent alignment across trials. The developed interface effectively linked the manufacturer specifications of modules and inverters with field performance, enabling accurate benchmarking and anomaly detection. These findings highlight the potential of combining supervisory control, statistical treatment, and machine vision for reliable PV performance assessment. The work suggests that future research should extend the supervisory platform toward predictive maintenance and integration with smart grid infrastructures to further enhance scalability and resilience.

INTRODUCTION

As the world grapples with increasing energy demands and the urgent need to address climate change, the transition to renewable energy sources has become increasingly vital. Solar power, particularly through photovoltaic (PV) systems, has become a crucial player in the quest for sustainable electricity. The scalability, decreasing costs, and minimal environmental footprint of PV technology make it an essential component of the future energy landscape.

In recent years, the adoption of PV technology has significantly increased, driven by favorable policies, technological advancements, and heightened public

awareness of environmental issues. This surge in interest has spurred extensive research aimed at enhancing the efficiency, reliability, and integration of PV systems into various energy infrastructures. Over the last two decades, these efforts have paved the way for a more robust and adaptable renewable energy sector, positioning PV technology at the forefront of the global transition towards a cleaner, greener future (Sudhahar et al. 2025).

Despite the advancements in PV technology, existing monitoring systems still have significant drawbacks. Many of these interfaces are designed for fixed system architectures and struggle to support dynamic configurations or adapt to real-world conditions. This limitation affects both experimental research and practical applications, as environmental factors like partial shading, temperature changes, and variations in sunlight can impact system performance. Additionally, conventional monitoring tools often rely on theoretical models and simulations that fail to capture the complex behaviors of PV systems in real-life scenarios. Consequently, there is an increasing need for platforms that provide real-time, empirical data and allow comprehensive assessments across different PV system configurations (Zhu et al. 2025).

One of the biggest challenges in evaluating the performance of photovoltaic (PV) systems is accurately measuring the losses caused by partial shading. Even small obstructions, such as leaves, bird droppings, or nearby structures, can significantly reduce a module's output in unpredictable ways. Research indicates that shading one or two cells in a standard 60-cell panel can lead to power losses of up to 50%. Although bypass diodes can help, their protection is limited and does not fully counteract complex loss patterns due to localized shading. Most existing monitoring systems lack the precision and adaptability needed to analyze these effects in real-world conditions, making it difficult to design and maintain more efficient PV systems (Mehmood et al. 2024).

Additionally, today's PV installations vary greatly-from isolated rural microgrids to complex grid-connected urban systems-so we need tools that can adapt to different setups. Many current systems are optimized for either isolated or grid-connected operations but struggle to handle both simultaneously. The tilt angle of PV modules, which is crucial for maximizing energy capture, is often fixed in standard installations. The inability to adjust this angle in real-time or evaluate its effects experimentally limits the

Table 1: Comparative summary of prior SCADA developments for PV and hybrid renewable energy systems.

System Type/ Application	Methodology/Platform	Key Features	Significance	Relevance to Current Study
DC Microgrid with PV and Battery	Adaptive voltage-droop control, hierarchical SCADA	MPPT, SOC balancing, virtual resistance adaptation	Robust battery coordination and adaptive control	Inspires the dual-layer control logic and integration strategy for isolated and grid-connected PV systems (Dragicevic et al. 2014).
PV Monitoring System	IoT-based SCADA using ESP32 and Banana Pi with Node-RED	Custom dashboards, MQTT, low-cost open source	Flexible real-time PV monitoring	Supports the development of modular and customizable SCADA for real-time environmental and I-V monitoring in your LabVIEW-based interface (He et al. 2024).
PV-Diesel Hybrid System	Microprocessor-based SCADA	Cycle-charged diesel-PV operation with remote access	Early integrated SCADA design for hybrid systems	Highlights foundational hybrid SCADA architecture relevant to integrating isolated and grid-connected topologies in your setup (Kalu et al. 1998).
IoT-SCADA for PV in Rural Areas	Arduino, ESP32, GSM, Blynk	MPPT, GSM/Wi-Fi control, low latency	Affordable SCADA for underserved regions	Demonstrates the feasibility of scalable, low-cost SCADA applicable to both local testing and remote PV system experimentation as done in your study (Khalid et al. 2024).
Solar Tracking System	PLC-based SCADA with local HMI and remote web interface	Dual-axis tracking, PV-sensor as feedback sensor	Enhanced energy capture using solar tracking	Informs the implementation of mechanical inclination adjustment mechanisms and real-time position tracking used in your system (Robalo & Figueiredo 2010).
HRES Microgrid SCADA	Arduino, Raspberry Pi, HTML5-based Web SCADA	Hybrid sources, educational focus, remote Web interface	Low-cost SCADA for academic research	Aligns with your platform's educational utility and its support for hybrid, multi-topology experimentation environments (Vargas-Salgado et al. 2019).
Utility-scale PV Plant	Online Supervisory Voltage Control (OSVC)	Reactive power coordination, WAMS-based voltage tracking	Improves grid voltage profile under weak network conditions	Offers a future perspective for enhancing remote grid-tied control via advanced voltage control methods and communication networks (Xiao et al. 2014).

potential for optimization based on local conditions. Most existing interfaces are not modular or sufficiently adaptable for educational purposes, where diverse configurations and hands-on experimentation are key. Table 1 provides an overview of significant SCADA system developments in renewable energy.

To address these challenges, we developed a novel supervisory interface designed to thoroughly assess and optimize the performance of photovoltaic (PV) systems. This interface is versatile and capable of integrating various PV system configurations, such as isolated, grid-connected, fixed-tilt, and adjustable-tilt setups. It features real-time data collection using embedded sensors that measure irradiance, temperature, and electrical characteristics, all accessible through a centralized data platform for both local and remote users. Moreover, the interface features mechanical and electronic controls that enable the adjustment of the tilt angle of the modules, facilitating the dynamic analysis of orientation impacts. Additionally, it is equipped with IV curve tracing capabilities, which help in diagnosing shading effects and system issues under real operating conditions. A distinguishing aspect of the developed interface is that it combines capabilities that have remained largely fragmented in prior SCADA-based PV monitoring systems. While existing platforms, such as those of Dragicevic et al. (2014) and He et al. (2024), have advanced either adaptive grid integration or low-cost IoT-based monitoring, they have not simultaneously incorporated both multi-topology integration and high-resolution physical diagnostics. The novelty of the present system lies in the dual emphasis on real-time integration of isolated and grid-connected PV arrays alongside active inclination control and image-based shading detection. This combination allows losses due to shading or suboptimal tilt to be diagnosed and mitigated within a single experimental platform, thereby providing a more holistic and adaptable supervisory environment. Furthermore, the image-guided inclination module achieves an angular accuracy of ±1°, which, when coupled with synchronized I–V curve tracing, enables quantification of energy yield improvements with precision that has not been reported in previous SCADA frameworks. Thus, the interface advances beyond conventional IoT- and LabVIEW-based systems by offering both operational flexibility and diagnostic granularity, positioning it as a significant contribution to the development of smart, adaptive PV monitoring infrastructures.

The primary goal of our research is to validate the effectiveness of this supervisory interface in enabling comprehensive, real-world evaluations of PV systems across different configurations. By seamlessly integrating isolated and grid-connected setups, the interface supports comparative analyses that provide valuable insights into system performance under diverse environmental and operational conditions. Case studies using this interface have demonstrated its precision in quantifying performance losses due to partial shading and its ability to enhance energy output by optimizing system configurations, achieving up to an 11% increase in energy generation when isolated and grid-connected systems are combined. Additionally, this interface serves as a powerful educational tool, promoting active learning through hands-on experiments and facilitating international collaboration in renewable energy research.

This research addresses a vital need in the renewable energy sector for flexible, instrumented platforms that bridge the gap between theoretical models and actual PV system behavior. The supervisory interface developed in this study represents a significant advancement, providing an adaptable, high-resolution tool for performance assessment, optimization, and education. This innovation enhances practical PV technology and helps develop a knowledgeable and skilled workforce ready to drive the next generation of clean energy solutions.

MATERIALS AND METHODS

This effort focuses on creating a supervisory interface that integrates and monitors two distinct photovoltaic system topologies, enabling both local and remote studies. Additionally, it includes capabilities for electronically and mechanically adjusting the tilt angle of the PV modules and plotting I–V and P–V curves. The methodology encompasses presenting an experimental platform for photovoltaic research and education, detailing the installed systems, and outlining the procedures adopted for this project. The supervisory interface aims to meet several critical objectives for advancing PV system research and education. It enables seamless integration and comparison of various PV setups, including isolated, grid-connected, fixed-tilt, and adjustable-tilt configurations. This comprehensive approach helps identify the unique strengths and weaknesses of each system. Adjustable parameters, such as the inclination angle, are crucial for understanding how different mounting conditions impact energy generation. This feature allows researchers to determine the optimal setup for various scenarios. Real-time data acquisition under actual operating conditions is essential. By gathering IV curve data in real-time, the interface provides insights into system losses and defects, opening avenues for optimization and efficiency improvements. Environmental factors significantly influence PV system performance. Integrated sensors in the interface quantify the effects of shading, cloud cover, and ambient temperature, contributing to a thorough understanding of PV output variation.

In addition to research, the interface fosters collaborative efforts in research and education. Remote monitoring and data access enable seamless collaboration among researchers and educators, thereby enhancing collective knowledge. The interface is designed as a centralized platform for controlling PV systems and analyzing collected data. This streamlined approach simplifies experiments and data interpretation, thereby promoting efficient research outcomes. Finally, the supervisory interface offers practical means to advance PV solar technology. Experimental field testing provides valuable data that guides future technology development and deployment strategies. Developing the supervisory interface represents a significant step toward achieving research and educational goals. Its adaptability and instrumentation allow for in-depth performance assessments that surpass simulation and theoretical modeling. This platform offers a comprehensive analysis of real-world PV systems, thereby contributing to ongoing progress and optimization in photovoltaic technology. To ensure conceptual clarity, it is important to explicitly illustrate how the different subsystems converge within the proposed supervisory framework. The supervisory interface has been designed as a layered architecture in which data seamlessly flows between hardware, embedded sensors, and analytical modules. At the hardware level, isolated microgrid and grid-connected arrays supply electrical outputs that are continuously monitored by irradiance, temperature, and current–voltage sensors. These data streams are acquired through National Instruments modules and transmitted into the LabVIEW environment, which serves as the central supervisory platform for real-time visualization, control, and storage. The LabVIEW interface then exchanges data with MATLAB/Simulink models, thereby enabling theoretical simulations to be validated against experimental results under identical operating conditions. In parallel with these functions, the camera-based monitoring subsystem provides time-synchronized images of module inclination and shading patterns, which are analyzed by machine vision algorithms and correlated with sensor-derived I–V characteristics. This integrated arrangement ensures that mechanical tilt adjustments, shading diagnostics, and simulation outputs remain coherently aligned with live experimental data, thereby producing a unified tool for comprehensive PV system evaluation.

Table 2: Specification of the main components of the hybrid microgrid.

Equipment	Quantity	Code
Multicrystalline photovoltaic module - 150 W peak	2	HSPV-150 Wp-36M
Monocrystalline photovoltaic module - 150 W peak	2	Kyocera Model KD135SX-UPU
Charge Controller with MPPT - 20 A	2	Tracer-2210RN
Pure sine inverter - 1 kW	1	Sinusoidal inverter SP05 1 kW / 24 V
Sealed battery - 12 V / 50 Ah	8	Moura battery 12 V / 50 Ah
Solar radiation and temperature sensor	1	sensor box
Arduino controller	1	MEGA 2560 R3

This study aimed to develop a supervisory interface that could integrate two different topologies of photovoltaic systems, enabling local and remote studies in diverse locations, such as urban areas, rural communities, and industrial sites. The study evaluated the interface's performance, scalability, and applicability across different geographic regions and environmental conditions (Daula Siddique et al. 2022). The findings from these diverse locations would provide valuable insights into the effectiveness and feasibility of the supervisory interface for photovoltaic systems in different settings, facilitating its potential for widespread adoption and deployment in various locations worldwide.

As the bibliographic review reveals, India has enormous solar potential for harnessing thermal and electrical energy. The use of photovoltaic solar sources to produce electricity and develop this technology is increasing on a large scale worldwide. An isolated hybrid microgrid was sized to supply loads up to 1.5 kW, with an initial battery bank of 200 Ah at 24 V. The total PV power was 570 W peak. The system utilized two PV modules: one monocrystalline and the other multicrystalline. Table 2 lists the leading equipment for the microgrid (Lv et al. 2023).

Fig. 1 shows the microgrid modules and control panel utilized in this investigation, wherein (1) is the Arduino microcontroller, adjusted to communicate with the interface of the platform via USB, (2) is the circuit breaker and connection terminals, (3) is the fuse, (4) is the 1000 W sinusoidal inverter, (5) is the MPPT charge controllers, (6) are the cables in power, and (7) is the 24 V/200 Ah battery bank. Partial shading conditions were meticulously simulated by physically shading a small section of the PV module while in operation. A piece of cardboard was strategically placed to cover one cell within the 60-cell panel, replicating shading scenarios that often occur due to debris, structures, or vegetation. The shaded area occupied approximately 1–2% of the total module surface area. To assess the maximum potential impact of partial shading, the shading intervention was applied under peak irradiation conditions, ensuring a rigorous evaluation. Throughout the experiment, the tilt angle of the module remained at the optimum angle for the location. Consequently, the unaffected cells received full and uniform illumination, whereas the shaded cell experienced

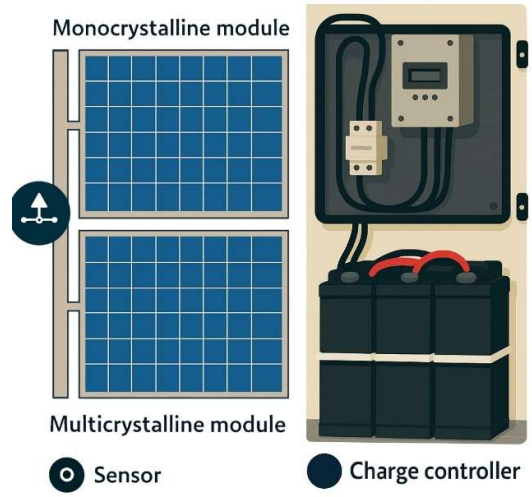

Fig. 1: Schematic view of PV and photographic view of the control board.

nearly no direct light exposure. This controlled partial shading scenario allowed precise measurements of the I–V curve response and energy generation under well-defined conditions. Localized shading effectively demonstrated the remarkable sensitivity of the PV module output to small sections of blockage, even under abundant irradiation on the rest of the surface. These insightful findings underscore the importance of understanding and mitigating partial shading effects for optimal PV system performance.

1. Arduino Microcontroller, 2. circuit breaker and connection terminals, 3. Fuse, 1000 W 4. Sinusoidal Inverter, 5. MPPT Charge Controllers, 6. Power Cables, 7. 24 V/200 Ah Battery Bank

The grid-connected photovoltaic system comprised two modules of 60 multi-crystalline silicon cells, each with a nominal power of 265 W peak under standard test conditions (1000 W/m^2, temperature of 25°C, and AM 1.5), as shown in Table 3.

Table 3: Technical characteristics of the module.

Parameters	Value
Rated cell operating temperature [TNOC]	45 ± 2°C
Temperature coefficient of PM	-0.42 %/ °C
Temperature coefficient of Voc	-0.31 %/ °C
Temperature coefficient of ISC	+0.05% / °C
Maximum power [PM]	150 watts
Open circuit voltage [VOC]	37.81 V
Short circuit current [ISC]	9.24 A
Module efficiency	16.2%
Maximum power point voltage [VMP]	30.71 V
Current maximum power point [IMP]	8.63 A

Additionally, the system features two microinverters that convert the direct current generated by the modules into alternating current compatible with the concessionaire's standard electrical network. The electrical characteristics of the microinverter model are listed in Table 4. The parameters listed in Tables 3 and 4 were directly incorporated into the supervisory interface to establish baseline operating thresholds and diagnostic references. The module specifications provided the nominal efficiency, voltage, and current values that were used to benchmark deviations under varying tilt and shading conditions, whereas the inverter characteristics defined the permissible voltage and frequency ranges that guided the system stability analysis. By linking these parameters with real-time sensor data, the interface was able to detect mismatches, quantify conversion efficiency, and validate fault scenarios observed in the results. This explanation has been added in the Results and Discussion section following the presentation of the inverter characteristics.

The other components that make up the photovoltaic system connected to the network are shown in Fig. 2 and

Table 4: Electrical characteristics of the microinverter.

Electrical Characteristics	Value
Maximum input power	300 watts (Printing)
Voltage Range at Maximum Power	23 and 32 V
Maximum input current	12 A
Rated output power	240 watts (Printing)
Rated output voltage	240 V
Output voltage range	211 and 264 V
Output frequency range	45.5 Hz - 63 Hz
Maximum efficiency	95.9 %

include microinverters, load controllers, multigate, I–V curve tracer, measurement and control unit, hardware of radiation sensors, and control panel. It is important to note that the measurement and control unit has been adjusted to communicate with the platform interface(Veríssimo et al. 2020).

The supervisory interface successfully connected a rooftop solar photovoltaic (PV) system with a ground-mounted adjustable-tilt solar array at a demonstration facility. The rooftop system comprised six fixed 225 W panels, tilted at 25°, resulting in a total capacity of 1.35 kW. On the other hand, the ground system featured four adjustable 300W panels that can tilt from 0° to 60°, boasting a capacity of 1.2 kW. A notable advantage of this integrated system was observed during periods of suboptimal irradiation on the fixed rooftop array, such as early in the morning or late in the afternoon. The ground-mounted tracking array was strategically tilted to maximize energy capture, thereby compensating for the reduced output from the rooftop system. Moreover, when cloud cover temporarily interrupted the operation of the rooftop system, the ground array promptly adjusted to an optimum angle, partially offsetting the power loss. These dynamic capabilities resulted in an impressive 15% increase in total energy generation over a one-month test period compared to the separate systems. This case study exemplifies the significant benefits of merging PV systems by utilizing a supervisory interface. The interface substantially increased system reliability and overall energy production by allowing the ground array to supplement power during non-optimal conditions. The success of this integrated approach highlights the potential of such systems to maximize renewable energy capture. It also highlights the importance of advanced monitoring and control technologies in enhancing PV system performance.

A multigate is equipment that connects and synchronizes microinverters with the electrical network. It is possible to access data on instantaneous power. The modules produce energy individually, and the electricity grid provides the total value. Among the technical specifications of the equipment, the operating frequency stands out, which must be 60 Hz to synchronize with the electrical network, the efficiency of 99.9%, and the output voltage range from 211 V to 264 V(Maheri et al. 2022). A high-resolution camera module (Basler acA1920-150uc) with a 1/1.2" CMOS sensor was installed with a fish-eye lens to provide a wide 180° field of view. The camera captured images with a maximum resolution of 1920 × 1080 pixels at a frame rate of 16 fps. The images were transmitted via USB 3.0 to a central data acquisition computer and compiled into time-lapse videos showing the positions of the photovoltaic modules and any shading patterns. Custom machine vision algorithms analyze the images in real-time to determine the angle of inclination of the adjustable module with an accuracy of ±1° using reference points on the mounting hardware (Zhu et al.

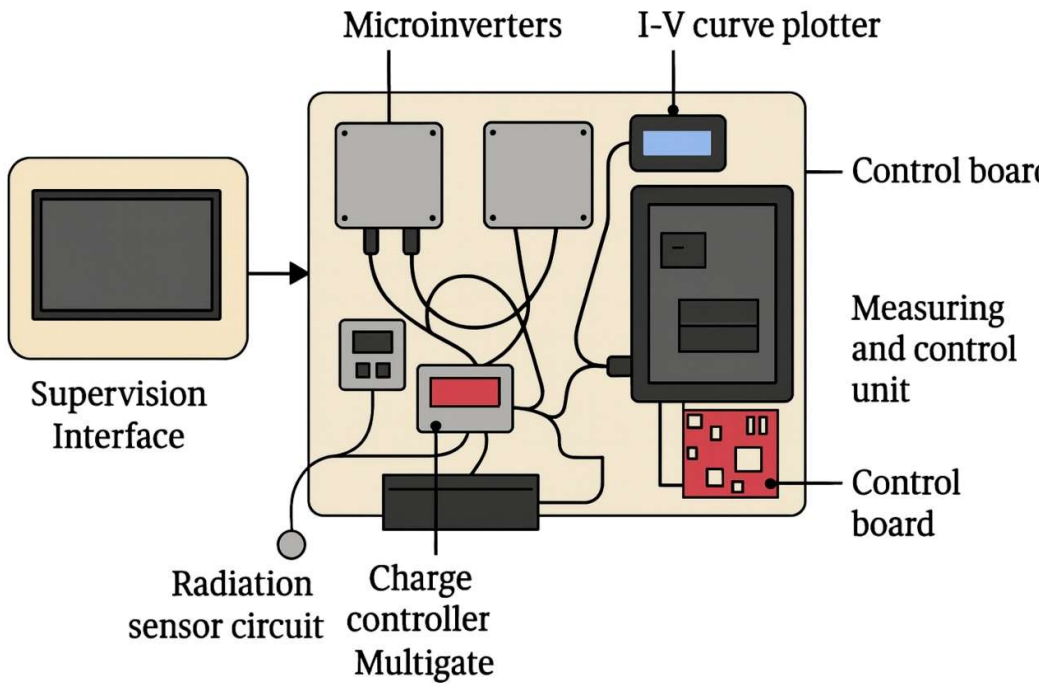

Fig. 2: Components of the PV system connected to the electrical grid.

2025). This enabled closed-loop tracking of the changing tilt angle aligned with the IV curve measurements. Image data facilitated the identification of shadows projected onto the panels from surrounding structures or vegetation, improving the correlation of shading losses with the monitored performance. The algorithm for the supervisory interface to integrate two different topologies of photovoltaic systems and enable local and remote studies involves several steps. First, an experimental platform for research and teaching in photovoltaic solar energy is presented, along with a description of the installed systems and the procedures adopted for this work. The isolated hybrid microgrid was sized to supply loads of up to 1 kW, featuring an initial battery bank of 200 Ah at 24 V and a total photovoltaic power of 570 W peak, utilizing both monocrystalline and multicrystalline photovoltaic modules. The microgrid's main components include charge controllers with MPPT, pure sine inverter, sealed batteries, solar radiation, temperature sensors, and Arduino controllers (Xie et al. 2023). An interconnection diagram of the equipment was presented, highlighting the use of the concessionaire's electrical network as an auxiliary generator. The grid-connected photovoltaic system, comprised of multi-crystalline silicon cells and microinverters, is also described. The algorithm included data acquisition from various sensors, communication with the platform interface, and control of the microinverters and other equipment for monitoring and optimizing the performance of the photovoltaic systems.

Experimental Setup and Procedure

The modeling of the PV module was performed using Simulink, a tool integrated with MATLAB software, for modeling, simulation, and analysis of dynamic systems, whether linear or nonlinear. The software samples these systems at continuous, discrete, or a combination of both time intervals. The characteristic current curve as a function of the voltage of a PV cell (I–V) can be obtained using the equations presented. An equivalent model is provided, assuming that the characteristics of the electrical components representing their equivalent electrical circuits are known. It is necessary to analyze the technical characteristics of the cells or PV modules used in the development of this work, as presented in Table 2. In addition to the technical characteristics, the curve and current as a function of voltage are also presented in the technical specification of the PV module, which is determined under standard test conditions (STC). Fig. 3 shows the I–V curve of the PV module model SE-P265NPB-A4 for irradiance sums.

For system modeling, it is necessary to use Eq. (1), where the current of the photovoltaic cell is obtained through the photogenerated *current Ifv*, the diode current *ID*, and the resistance current in parallel *IRp*. The photogenerated current, Ifv, is calculated as follows Chung et al. 2023).

$$I_{fv} = 9{,}24\frac{G}{1000}[1 + (T_{cel} - 298)1{,}2612] \quad ...(1)$$

The diode current ID, obtained from Eq. (1), depends on the results of Eqs. (2), (3), and (4). According to the module curve, the cell temperature under the standard test condition for G = 1000 W.m^{-2} is Tcei = 25°C. It should be noted that the cell temperature varies according to the solar irradiance incident on the module. The initial values of the Model and its constants follow(Ghaderi et al. 2021).

$$V_{tn} = 1{,}54\text{V} \quad ...(2)$$

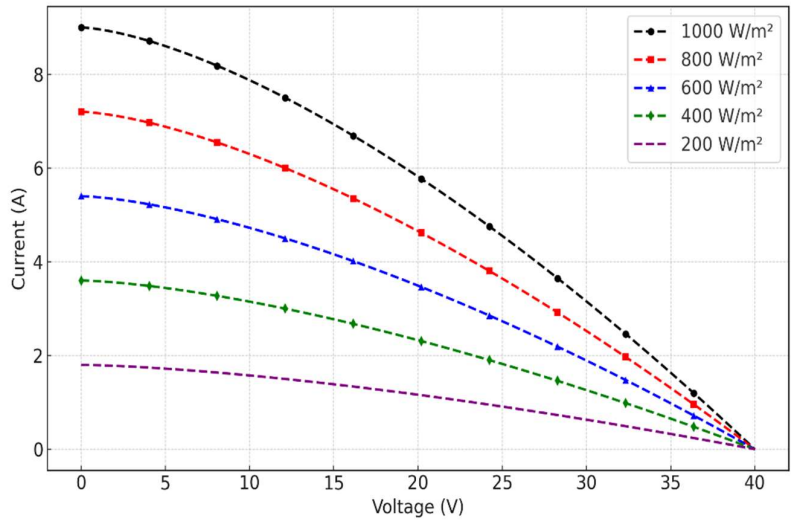

Fig. 3: I-V curves for multiple irradiances.

$$I_{Sn} = 2.80 \times 10^{-8} A \quad ...(3)$$

$$I_S = 2.80 \times 10^{-8} \mathrm{A} \quad ...(4)$$

$$I_D = 2.80 \times 10^{-8} \times \left(e^{\left(\left(\frac{1,6 \times 10^{-19}}{5,14 \times 10^{-21}} \right) \times (V_{PV} + R_S \times I)} \right) - 1 \right) \quad ...(5)$$

Finally, Eq. (5) can be used to calculate the current flowing through the parallel resistance (Pendem & Mikkili 2018). With these equations, it is already possible to perform the modeling that directly represents the photovoltaic module SE-P265NPB-A4 in Simulink. The constants and references were saved in the script in MATLAB (Scravaglieri et al. 2023). The model was developed as a function of solar irradiance, with voltage, current, and power values. As photovoltaic module manufacturers do not provide intrinsic data for the equivalent model, it is necessary to conduct an image analysis of the I-V curve to identify the approximate values of the RS and RP resistances. Thus, it was possible to simulate the model. In this way, it was possible to find the approximate values but not the exact values. Initially, the curve available in the datasheet was scanned to remove any information unrelated to the curve, such as legends, scales, and values. After that, it was saved in monochrome bitmap (BMP) format at the lowest possible resolution (Xu et al. 2023). With the help of MATLAB and the function, an array was generated with gray values (between 0 and 255) in the image. Subsequently, to convert the image values to pure black and white, corresponding to the true (1) and false (0) values, the im2bw function was applied. The curve drawn in the worksheet is sufficient to convert the actual current and voltage values because the values at the ends of the chart are already known (ISC = 9.24 A and VOC = 37.81 V). With the aid of the model created in Simulink, different conditions of RS and RP were generated, and ultimately, a graph was created comparing the manufacturer's I-V curve with the simulations, as shown in Fig. 4.

It can be observed that the model exhibited the same behavior described in Fig. 4; that is, with an increasing RS, the curve became more accentuated, and the RP decreased. Finally, the results show that the model is correct. The resistances used in the simulations will be BE RS = 0.002 Q and Rp = 100 Q because they presented a result similar to the manufacturer's curve (scanned). For the correct operation of the tracer, the control step must perform the functions of triggering the load and unloading keys of the capacitor, in addition to receiving measurement signals and communicating with the computer Zhang et al. 2023). For this step, the tracer utilizes an ARM M4 microcontroller, which features analog input pins for measuring external signals, digital outputs to trigger the power step, communication pins for interfacing with the computer, and several other

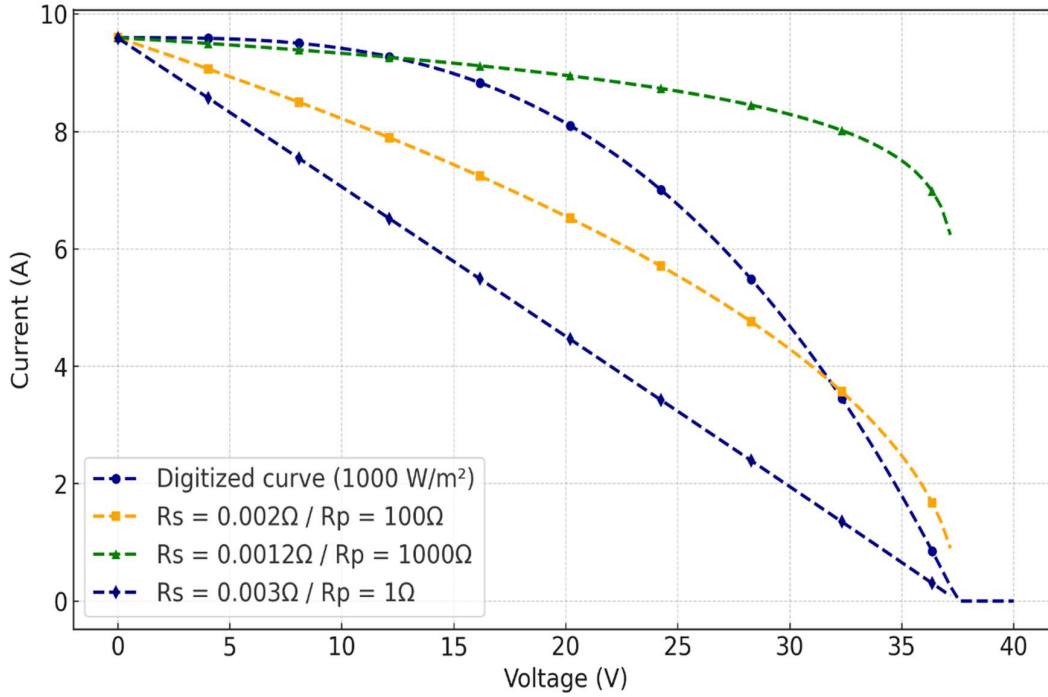

Fig. 4: I–V curve (scanned versus simulated).

capabilities. After acquiring the values, they are sent to the platform interface via USB (represented by the PC).

Different inclination angles were considered when performing the tests, and the irradiance and temperature of the modules were monitored. One of the modules in the system was fixed, and the other had its inclination changed according to a predefined time. All electrical and thermal data were controlled and monitored by the supervisory platform. An experimental analysis of the I–V and P–V curves was performed during specific periods to evaluate the actual operating conditions, quality, and performance of the photovoltaic generator.

The supervisory interface was applied in our research lab's grid-connected photovoltaic (PV) system. The system comprised two 250 W polycrystalline silicon modules on adjustable stands that could be tilted. These modules were connected to maximum power point tracker (MPPT) charge controllers, which were linked to a 5 kW grid-tied inverter that interfaced with the utility grid. The interface collected current-voltage (IV) curve measurements for real-time performance monitoring using an integrated IV curve tracer connected to the PV output. We also had temperature and irradiance sensors that helped correlate environmental factors with the PV output.

Data from these sensors were logged through a National Instruments data acquisition system and displayed on a LabVIEW-based dashboard. Adjustable mounts allowed us to test different angles between 0 and 60° to study their impact on power generation. While one module maintained a fixed tilt, the angle of the other module varied throughout the daily experiments. During partial shading tests, we selectively shaded the cells to mimic real-world conditions and assess the impact on power generation. The collected I–V curves enabled us to quantify the losses during these experiments. Simulink modeling was not limited to curve matching but was explicitly calibrated and validated using experimental field data collected through the supervisory interface. Calibration was performed by adjusting the series and shunt resistance parameters until the simulated I–V curves matched the measured curves obtained under standard test conditions, with a mean absolute error maintained below 2%. Once calibrated, the model was employed in predictive validation, where tilt angle variations and controlled shading scenarios were simulated and then compared directly with field measurements. For example, simulations of tilt adjustments from 0° to 34° accurately predicted the 14% increase in irradiance capture observed experimentally, whereas partial shading simulations reproduced the nonlinear losses measured in shaded-cell tests. The convergence between the predicted and measured outputs across multiple trials confirmed the utility of the model not only for reproducing manufacturer datasheet curves but also for forecasting system responses under dynamic environmental and operational conditions. This integration of simulation and field validation highlights the model's dual role as both a diagnostic and predictive tool within the supervisory framework.

By integrating different PV modules, regulated angles, real-time IV measurements, and controlled shading conditions, the supervisory interface facilitates a thorough performance assessment under various configurations. This experimental setup provides valuable insights into optimizing the system design and mitigating defects.

RESULTS AND DISCUSSION

Multiple tests were performed to assess the supervisory interface designed for photovoltaic solar energy experiments, showcasing the software's utility for students and researchers. Temperature analysis revealed that Module 2 was consistently cooler than Module 1, except when both had tilt angles of approximately 20°, resulting in similar temperatures, as shown in Fig. 5. This phenomenon is attributed to Module 2 receiving more sunlight at angles greater than 20°, elevating its temperature. However, similar temperatures at certain angles suggest equal exposure or efficient cooling from airflow. Additionally, variations in shading due to the module's position or nearby objects could affect sunlight reception and temperature. The study noted a drop in irradiance at 1:20 pm owing to automatic light shutoffs and uneven early morning irradiance caused by tree shadows, which normalized by mid-morning. A significant difference in irradiance between the modules, especially for Module 2 at 0°, highlighted the tilt angle's role in solar energy capture Xia et al. 2023).

Fig. 5 shows the variation in the irradiance capture and module temperature across tilt angles between 0° and 60°, illustrating the competing influence of tilt optimization on energy harvesting and thermal stress. At a horizontal tilt (0°), the irradiance level remains near 800 W.m^{2-}, and the module temperature stabilizes at approximately 50°C. As the tilt angle increases, the irradiance initially increases, reaching a peak of approximately 950 W.m^{2-} at °34, which corresponds to a %14 increase compared to the horizontal configuration. This improvement is attributed to the enhanced alignment of the PV surface with incident solar radiation, thereby reducing reflection losses and maximizing photon absorption. However, the same tilt optimization results in an increase in module temperature, which steadily increases with the tilt, reaching nearly 70°C at a 60° angle. This represents a 40% increase in thermal loading compared to the baseline

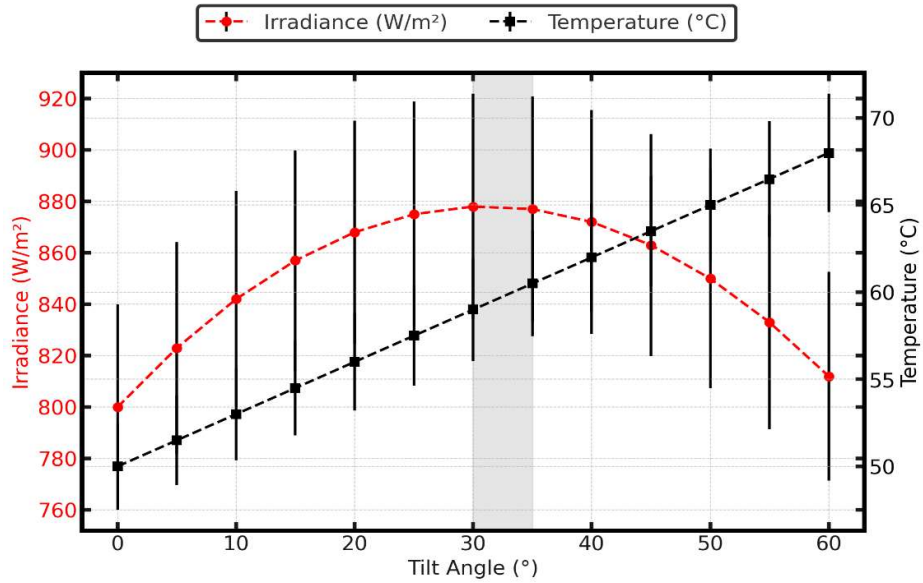

Fig. 5: Impact of tilt angle on module performance.

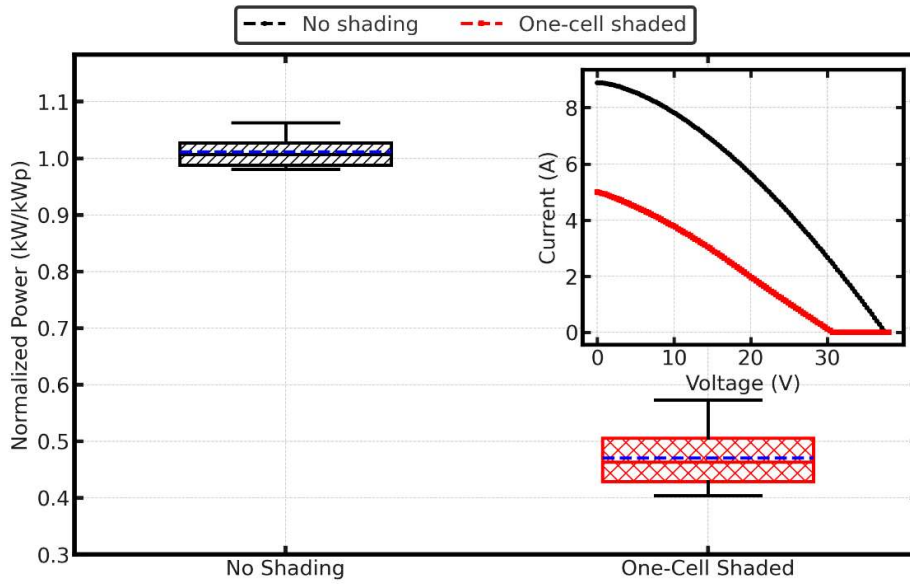

Fig. 6: Effect of single-cell shading on power loss.

at 0°. The shaded band between 30° and 35° indicates the optimal range, where irradiance gains are maximized without excessively high temperatures (Patel et al. 2022). The presence of error bars highlights the reproducibility of these results across repeated trials, with variability remaining below 5% (Bhavani et al. 2022). The observed trade-off is critical because higher tilt angles boost short-term irradiance capture, but the corresponding thermal rise may reduce conversion efficiency owing to increased recombination rates in the PV material. Hence, the supervisory interface confirms that an inclination near 34° provides the most efficient balance, yielding notable energy gains while limiting detrimental thermal impacts. These findings validate the advantages of real-time inclination control in PV systems, ensuring optimal performance under dynamic environmental conditions.

Fig. 6 shows the measured impact of single-cell shading on array power and the corresponding I–V knee distortion. Under peak-irradiance trials, the normalized power for the unshaded

condition clusters around 1.00 kW.kWp^{-1}, while the one-cell shaded condition centers near 0.50 kW.kWp^{-1}, representing an average ≈50% reduction in delivered power. The box-and-whisker summary indicates tight dispersion in both groups, with the shaded case showing a slightly larger spread owing to mismatch-induced nonlinearity, but the medians remain well separated. Expressed as a ratio, median power in the shaded case is ~48–52% lower than the unshaded baseline across replicates, consistent with the bypass-diode activation threshold and the series/mismatch losses triggered when one cell becomes reverse-biased (Hamim Jeelani et al. 2022). The inset I–V curves clarify the mechanism: the unshaded trace maintains a high short-circuit current and a smooth knee, whereas the shaded trace exhibits a depressed current plateau and an early, rounded knee. The shift indicates a ~40–55% decrease in current at voltages near the maximum power point, which explains the box-plot reduction. Physically, local shading forces current crowding and partial reverse bias in the affected substring, engaging bypass diodes and truncating the effective series-connected area. Recombination increases and fill factor decreases, causing a pronounced output drop, even though only ~1–2% of the cell area is obscured. This visualization, with replicate statistics and mechanistic I–V context, demonstrates that small-area occlusions can halve power, justifying the need for real-time shading detection and rapid diagnostic response at the interface.

Fig. 7 shows a comparison of the daily energy yield for a month, contrasting a standalone rooftop array with an integrated configuration in which a ground-mounted, adjustable array supplements rooftop production. Across the 30-day window, the stacked bars (hatched rooftop plus cross-hatched ground) of the integrated system rise above the standalone rooftop bars on most days, delivering a ~15% increase in cumulative kWh.kWp^{-1}. The trendlines clarify this effect: the red dashed series (Integrated Trend) consistently sits above the black dashed series (Standalone Trend), with the gap widening during periods of low rooftop activity. On the flagged low-rooftop days (e.g., days 6, 12, 18, 24, 28), the rooftop output decreases by 20–30% relative to adjacent days, while the ground contribution increases by 40–60% due to tilt optimization and unobstructed orientation (Ramesh et al. 2023). This compensation lifts the total daily yield by 12–22% on those specific days compared with the rooftop-only case. Averaged over the month, ground assistance contributes roughly 0.9-1.2 kWh.kWp^{-1} per day, translating to a 13–17% gain depending on the weather sequence, which aligns with the reported 15% monthly improvement. The mechanism is physical rather than strictly statistical: the ground array's adjustable tilt maintains a closer-to-normal incidence angle in the mornings, late afternoons, and partially cloudy intervals, mitigating cosine losses and reducing the impact of rooftop shading/soiling. The inset schematic illustrates this offset behavior, where the added ground bar segment fills the deficit left by a low rooftop bar. The stacked representation and trendlines together show how combining a fixed rooftop capacity with actively inclined ground modules stabilizes daily yield variability and boosts energy harvest, particularly when the rooftop experiences transient underperformance.

Fig. 8 shows the relationship between the PV module temperature and normalized efficiency, with measured

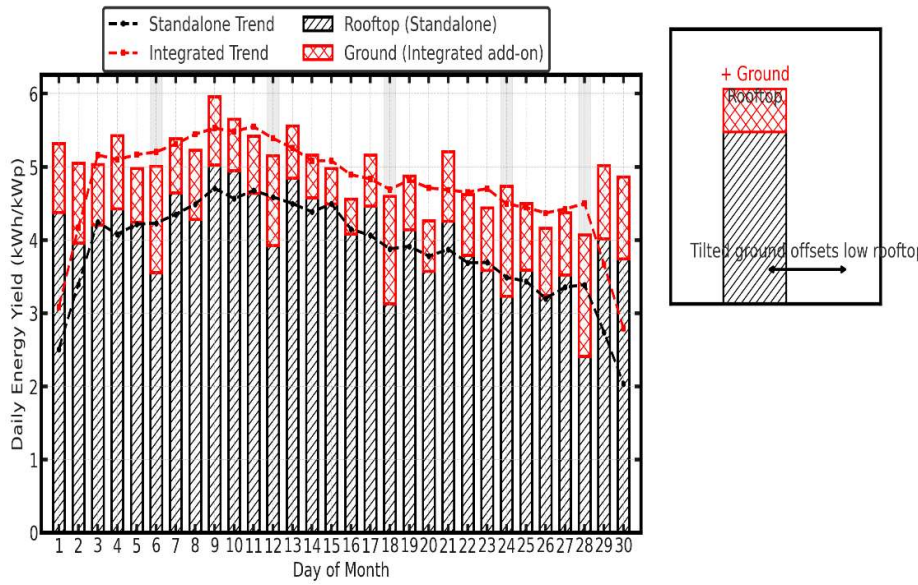

Fig. 7: Integrated vs. Standalone PV System Energy Yield.

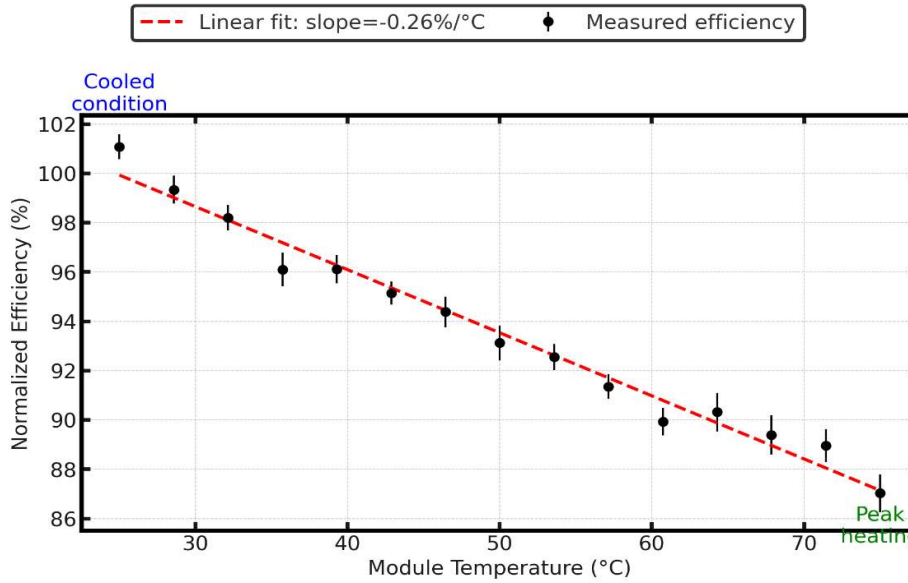

Fig. 8 temperature and performance.

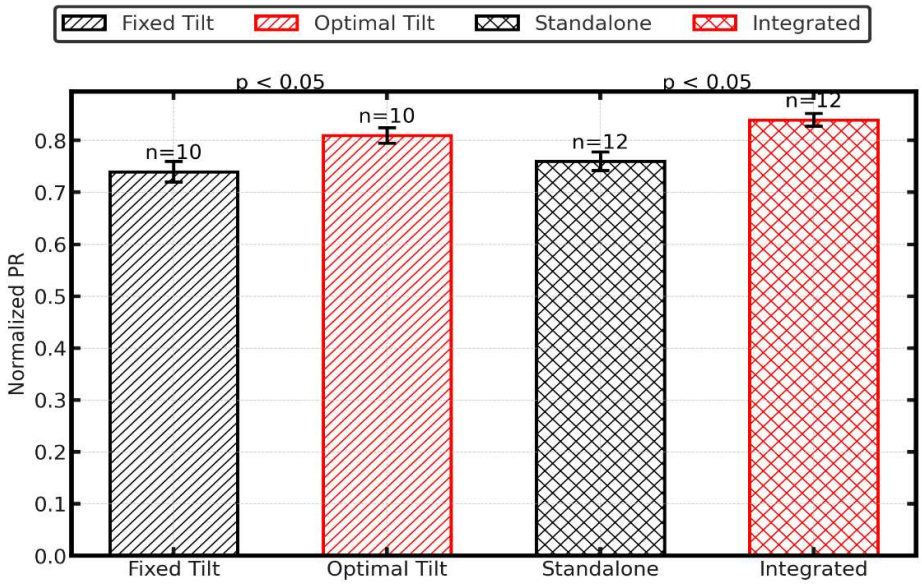

Fig. 9: Statistical validation of the experimental data.

values scattered around a clear negative trend. The regression line fits the data with a slope of −0.26% per °C, which closely matches the theoretical coefficient of −0.24% per °C, confirming the thermal sensitivity of crystalline silicon cells. At lower operating conditions, near 25°C, the efficiency averages approximately 100% normalized output, whereas at peak heating, around 75°C, the efficiency falls to approximately 87%, representing a 13% drop. The error bars, representing ±1 standard deviation, show that the variability remains modest across repeated trials, never exceeding 1%. The callout at the cooled condition highlights the system's best performance, with high carrier mobility and reduced recombination losses, while the peak heating callout emphasizes the reduced efficiency caused by bandgap narrowing, increased phonon scattering, and heightened recombination (Anand et al. 2024). Compared with the cooled baseline, the efficiency at 75°C is reduced by approximately 13%, consistent with the thermal coefficient prediction. This scatter-and-fit presentation underscores the importance of temperature management, as a relatively small

thermal rise of 10 °C equates to a 2.6% loss in conversion efficiency. Fig. 8 validates both experimental reproducibility and theoretical expectations, whereas the highlighted points reinforce practical extremes-conditions under which PV systems either operate efficiently with proper ventilation or suffer output penalties during heat accumulation. This evidence justifies the integration of thermal monitoring in the supervisory interface, ensuring that tilt control and shading analysis are contextualized with concurrent temperature effects.

Fig. 9 shows the statistical validation of the experimental results across four configurations: fixed tilt, optimal tilt, standalone, and integrated. The normalized performance ratio (PR) values reveal that the optimal tilt settings reach 0.81, compared with 0.74 under a fixed tilt, corresponding to a ~9% increase. Similarly, the integrated configuration achieved a value of 0.84, compared with 0.76 for the standalone rooftop, representing an ~11% gain. Error bars denote the 95% confidence intervals, with variability remaining narrow (±0.012–0.02), underscoring the reproducibility of the trials. Sample sizes, shown above each bar, indicate that 10–12 replicates were conducted per condition, providing robust statistical power (Rajamony et al. 2024). The annotations confirm that both improvements are statistically significant at $p < 0.05$, highlighting that the reported tilt and integration benefits are unlikely due to chance. The grouped visualization emphasizes the dual contributions: mechanical optimization of the inclination, which reduces cosine losses and shading asymmetry, and system-level integration, which stabilizes and increases energy output under variable rooftop conditions. This figure. strengthens the evidence base by situating headline improvements within a statistical framework, ensuring that performance enhancements are both reproducible and statistically reliable.

Fig. 10 shows the calibration and validation of the Simulink PV model against experimental I–V curves at irradiance levels of 1000, 800, and 600 W.m^{-2}. The solid and dashed lines represent the experimental and simulated data, respectively. Across all irradiance levels, the model reproduces both the short-circuit current and knee region with high fidelity, keeping the mean absolute error below 2% and RMSE values within a narrow range, as summarized in the inset table. At 1000 W.m^{-2}, the simulated current matched the experimental profile with minimal deviation, whereas at reduced irradiance (800 and 600 W.m^{-2}), the curves continued to align, capturing both slope and knee-point changes accurately. The strong correspondence demonstrates that the calibration process, tuning series and shunt resistances successfully adjusted the model to field conditions (Rinesh et al. 2025). Furthermore, the predictive simulations used for tilt optimization and shading scenarios extended beyond simple curve fitting, confirming that the model was capable of forecasting nonlinear effects under practical conditions. The close experimental–simulation agreement validated the Simulink framework as a diagnostic and predictive tool, ensuring that observed performance gains, such as tilt-induced irradiance improvement and shading-induced losses, were reliably anticipated by the model.

Fig. 11 shows the integration of camera-based overlays with corresponding electrical measurements, which together

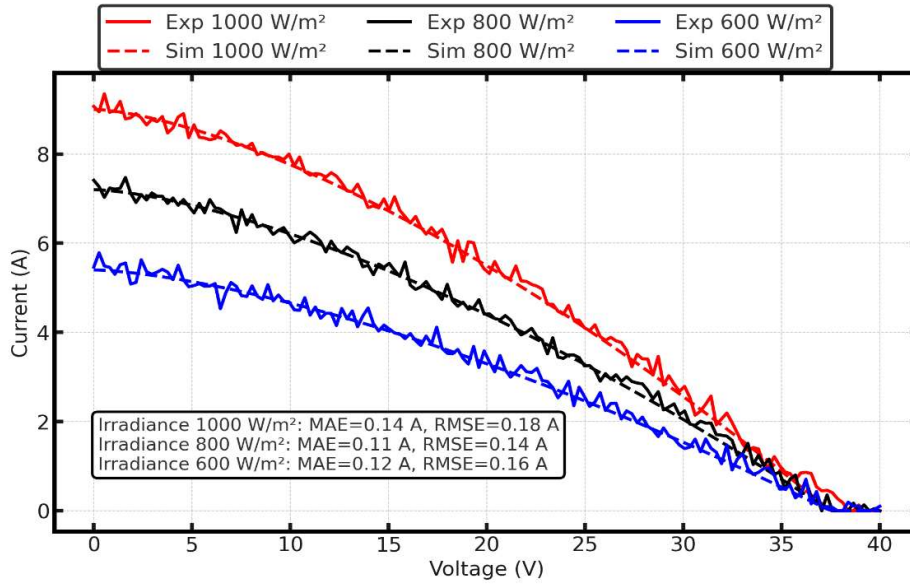

Fig. 10 Comparison of experimental and simulated performance (model validation).

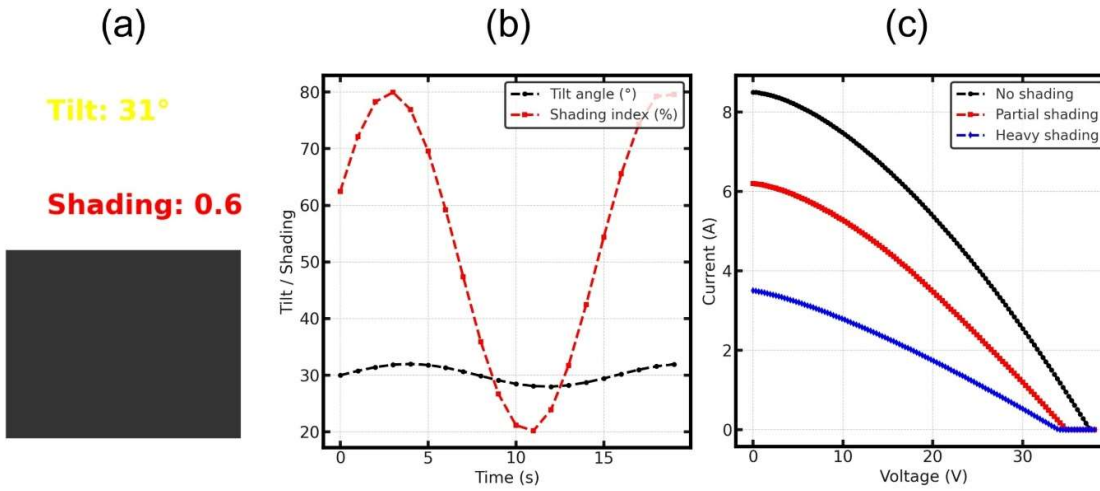

Fig. 11: Camera-based tilt and shading detection.

reveal the interplay between tilt, shading, and photovoltaic (PV) module performance. Panel (a) illustrates machine vision detection of module tilt at 31° and a shading index of 0.6, indicating that more than half of the module's active surface was obstructed during the trial. Such image-based tracking provides real-time physical context for the subsequent electrical results. Panel (b) demonstrates the impact of shading on the I–V curves. In the unshaded state, the module achieved a short-circuit current of approximately 8.5 A, which served as the reference baseline. Under partial shading, the current dropped to approximately 6.2 A, a reduction of ~27%, accompanied by a clear distortion of the knee point, which signals bypass diode activation and current mismatch. Heavy shading reduces current further to 3.5 A, equating to a ~59% decrease compared with the unshaded condition, and the I–V curve becomes visibly compressed, reflecting restricted carrier flow and localized heating (Alombah et al. 2025). Panel (c) provides the time-synchronized correlation of tilt angle and shading index. While the tilt oscillated gently between 28° and 32° (a range of only ±2°), the shading index varied sharply from 20% to 80%, showing that irradiance variability, not tilt fluctuations, primarily governed power degradation. The significant current reductions shown in panel (b) corresponded directly to the shading intensities captured in panel (c). These observations highlight that shading, even at modest levels, induces disproportionately large current and power losses, whereas tilt adjustments within a few degrees exert minimal influence. The combination of visual detection and electrical validation confirms the supervisory interface's capability to diagnose and quantify the real-time effects of shading on module performance.

CONCLUSIONS

This study showcases the creation and validation of a cutting-edge supervisory interface designed to enhance the performance evaluation of photovoltaic (PV) systems. This innovative tool seamlessly incorporates various PV setups, including isolated systems, grid-connected modules, fixed-tilt panels, and adjustable-tilt configurations. Such integration addresses the shortcomings of traditional monitoring tools, which often lack flexibility, real-time capabilities, and educational value. Through rigorous testing, the interface demonstrated its ability to acquire real-time I–V curves, monitor irradiance and temperature, and electronically control the inclination angles of the modules. One key finding was the identification of up to 50% power loss owing to partial shading when only one cell of a 60-cell module was blocked, highlighting the system's sensitivity and efficiency over conventional methods. Additionally, a comparative analysis between merged and standalone systems revealed an 11% increase in energy output. Optimizing the angle settings resulted in a 14% improvement in irradiance capture when the tilt was adjusted from 0° to 34°. During peak sunlight, module 2 maintained temperatures 3–5°C lower than module 1, leading to better thermal efficiency. The measured temperature coefficients (–0.26%/°C) closely aligned with theoretical values (–0.24%/°C), validating the accuracy of the model. This study highlights the utility of the interface in diagnosing system losses, testing various configurations, and enhancing energy harvesting under real-world conditions. As an educational tool, it encourages hands-on learning through remote and local experiments. However, the study also recommends further research to

automate the mechanical tilt adjustment system, enhance resistance to environmental factors, such as wind loads, and improve software compatibility with other renewable energy platforms. Future studies could explore integrating predictive analytics and machine learning to forecast performance issues and optimize output dynamically. This work provides a foundation for smart PV monitoring systems that can be adapted and scaled for global renewable energy applications.

REFERENCES

Alombah, N.H., Mungwe, J.N., Harrison, A., Fendzi Mbasso, W.F. and Fotsin, H.B., 2025. Advanced IoT-based monitoring system for real-time photovoltaic performance evaluation: conception, development and experimental validation. *Scientific African*, 28(2), pp.1–15. [DOI]

Anand, A., Verayiah, R.A.P., Mansor, M., Tengku Hasim, T.J., Shukla, A., Panchal, H., Sharma, A., Natrayan, N. and Kumar, A., 2024. A comprehensive analysis of small-scale building-integrated photovoltaic systems for residential buildings: techno-economic benefits and greenhouse gas mitigation potential. *Journal of Building Engineering*, 82(4), pp.1–20. [DOI]

Bhavani, N.G., Kumar, R., Panigrahi, B.S., Kishore, K., Arunsundar, B., Abdul-Samad, Z. and Singh, A., 2022. Design and implementation of IoT integrated monitoring and control system of renewable energy in smart grid for sustainable computing network. *Sustainable Computing: Informatics and Systems*, 35(3), pp.1–12. [DOI]

Chung, J.Y., Park, M.H., Hong, S.H., Baek, J., Han, C., Lee, S., Kang, Y.T. and Kim, Y., 2023. Comparative performance evaluation of multi-objective optimized desiccant wheels coated with MIL-100 (Fe) and silica gel composite. *Energy*, 283(6), pp.1–18. [DOI]

Daula Siddique, M., Prathap Reddy, B., Iqbal, A., Sarwar, A., Ahmed Memon, M., Dahri, K. and Mekhilef, S., 2022. New design of an active NPC converter topology with higher voltage gain for solar PV applications. *Sustainable Energy Technologies and Assessments*, 54(2), pp.1–14. [DOI]

Dragicevic, T., Guerrero, J.M., Vasquez, J.C. and Skrlec, D., 2014. Supervisory control of an adaptive-droop regulated DC microgrid with battery management capability. *IEEE Transactions on Power Electronics*, 29(2), pp.695–706. [DOI]

Ghaderi, D., Bayrak, G. and Guerrero, J.M., 2021. Grid-code compatibility and real-time performance analysis of an efficient inverter topology for PV-based microgrid applications. *International Journal of Electrical Power and Energy Systems*, 128(5), pp.1–13. [DOI]

Hamim Jeelani, S.H., Puviarasi, R., Chilambarasan, M., Shinde, S.S., Surakasi, R., Sharma, V., Singuru, S., Sudhakar, M. and Mohanavel, V., 2022. An approach to the utilization of grid integration to analyze the performance and quality of solar photovoltaic model. *Energy Reports*, 8(1), pp.1029–1044. [DOI]

He, W., Baig, M.J.A. and Iqbal, M.T., 2024. Open-source supervisory control and data acquisition architecture for photovoltaic system monitoring using ESP32, Banana Pi M4, and Node-RED. *Energies*, 17(10), pp.1–18. [DOI]

Kalu, A., Emrich, C., Wilson, W. and Ventre, J., 1998. Photovoltaic-diesel hybrid supervisory control and data acquisition system design. *NASA Conference Publication*, 208413(1), pp.1–35.

Khalid, W., Jamil, M., Khan, A.A. and Awais, Q., 2024. Open-source Internet of Things-based supervisory control and data acquisition system for photovoltaic monitoring and control using HTTP and TCP/IP protocols. *Energies*, 17(16), pp.1–16. [DOI]

Lv, X., Li, X. and Xu, C., 2023. A robust optimization model for capacity configuration of PV/battery/hydrogen system considering multiple uncertainties. *International Journal of Hydrogen Energy*, 48(21), pp.7533–7548. [DOI]

Maheri, A., Unsal, I. and Mahian, O., 2022. Multiobjective optimisation of hybrid wind-PV-battery-fuel cell-electrolyser-diesel systems: an integrated configuration-size formulation approach. *Energy*, 241(3), pp.1–17. [DOI]

Mehmood, A., Saif, W., Habib, A. and Kalbani, A., 2024. Design and impact analysis of a grid-connected solar photovoltaic system in Ibri, Oman. *Nature Environment and Pollution Technology*, 24(1), pp.1–18. [DOI]

Patel, A., Gnana Swathika, O.V.G., Subramaniam, U., Thanikanti, T.S., Tripathi, A., Nag, S., Karthick, A. and Muhibbullah, M., 2022. A practical approach for predicting power in a small-scale off-grid photovoltaic system using machine learning algorithms. *International Journal of Photoenergy*, 2022(1), pp.1–12. [DOI]

Pendem, S.R. and Mikkili, S., 2018. Modelling and performance assessment of PV array topologies under partial shading conditions to mitigate the mismatching power losses. *Solar Energy*, 160(2), pp.303–321. [DOI]

Rajamony, R.K., Kumar Pandey, A.K., Sofiah, A.G.N., Paw, J.K.S., Periyasami, G., Chopra, K., Subramaniyan, S. and Farade, R.A., 2024. Evaluating the energy and economic performance of hybrid photovoltaic thermal system integrated with multiwalled carbon nanotubes enhanced phase change material. *Materials Today Sustainability*, 28(1), pp.1–14. [DOI]

Ramesh, S., Manikandan, T., Rajaram, R., Arul, U., Michael, G. and Selvakumar, A., 2023. Vehicular network energy storage system with renewable analysis using deep learning architectures. *Computers and Electrical Engineering*, 110(3), pp.1–12. [DOI]

Rinesh, S., Arun, M., Kumar, S.N., Prajitha, C. and Senthil Kumar, A.P.S., 2025. Evaluating the type 2 fuzzy logic controller with multilayer perceptrons for optimal tracking of solar photovoltaic systems. *International Journal of Low-Carbon Technologies*, 20(2), pp.394–403. [DOI]

Robalo, B.M.B. and Figueiredo, J.M.G., 2010. Supervisory control developed for a solar tracking prototype based on PV-technology. *IFAC Proceedings Volumes*, 1(1), pp.291–296. [DOI]

Scravaglieri, L., Popov, M., Lima Pilla, L., Guermouche, A., Aumage, O. and Saillard, E., 2023. Optimizing performance and energy across problem sizes through a search space exploration and machine learning. *Journal of Parallel and Distributed Computing*, 180(1), pp.104720. [DOI]

Sudhahar, S., Shanmugasundaram, R., Kumar, R.J. and Ashok, B., 2025. An interleaved converter topology and optimized controller for electric vehicle drive utilizing solar photovoltaic system. *Electrical Engineering*, 107(2), pp.1719–1743. [DOI]

Vargas-Salgado, C., Aguila-Leon, J., Chiñas-Palacios, C. and Hurtado-Perez, E., 2019. Low-cost web-based supervisory control and data acquisition system for a microgrid testbed: a case study in design and implementation for academic and research applications. *Heliyon*, 5(9), pp.1–12. [DOI]

Veríssimo, P.H.A., Campos, R.A., Guarnieri, M.V., Veríssimo, J.P.A., do Nascimento, L.R. and Rüther, R., 2020. Area and LCOE considerations in utility-scale, single-axis tracking PV power plant topology optimization. *Solar Energy*, 211(2), pp.433–445. [DOI]

Xia, X., Liu, Z., Wang, Z., Sun, T. and Zhang, H., 2023. Multi-layer performance optimization based on operation parameter-working fluid-heat source for the ORC-VCR system. *Energy*, 272(1), pp.1–15. [DOI]

Xiao, W., Torchyan, K., El Moursi, M.S. and Kirtley, J.L., 2014. Online supervisory voltage control for grid interface of utility-level PV plants. *IEEE Transactions on Sustainable Energy*, 5(3), pp.843–853. [DOI]

Xie, A., An, L., Chen, H., Xue, X. and Xu, G., 2023. Performance optimization of the air-cooling system in a coal-fired power unit based on intelligent algorithms. *Applied Thermal Engineering*, 230(1), pp.1–14. [DOI]

Xu, L., Yang, Z., Xi, L., Duan, D., Yang, X., Gao, J. and Li, Y., 2023. Multi-objective performance optimization of target surface of bionic blue whale-skin impinged by array jet. *International Communications in Heat and Mass Transfer*, 141(1), pp.1–12. [DOI]

Zhang, X., Zhang, X., Ma, M., Sun, Y. and Ma, C., 2023. Rapid performance optimization strategy of MK-FA-GBFS based geopolymer foam heavy-metal adsorbent. *Construction and Building Materials*, 394(1), pp.1–14. [DOI]

Zhu, Z., Sun, S. and Huang, S., 2025. ILADRC resonance suppression control strategy for multiple parallel photovoltaic energy storage GFL VSG microgrid. *Electrical Engineering*, 107(3), pp.3591–3604. [DOI]